Long-term Growth and Subsidence of Ascension Island: Constraints on the Rheology of Young Oceanic Lithosphere

T. A. Minshull[1*], O. Ishizuka[2] and D. Garcia-Castellanos[3]

[1]National Oceanography Centre Southampton, University of Southampton, European Way Southampton SO14 3ZH, UK

[2]Institute of Geology and Geoinformation, Geological Survey of Japan/AIST Central 7, 1-1-1 Higashi, Tsukuba, Ibaraki 305-8567, Japan

[3]Institute of Earth Sciences Jaume Almera, Lluis Solé i Sabaris s/n, Barcelona, Spain

Corresponding author email: tmin@noc.soton.ac.uk

The dating of material from deep boreholes drilled in volcanic ocean islands allows constraints to be placed on their growth and long-term subsidence rates. We dated lavas from a 3 km geothermal borehole at Ascension Island by the laser-heating $^{40}Ar/^{39}Ar$ technique. The samples yield ages of up to 3.4 Ma and volcanic growth rates of ~0.4 km/Myr. The transition from submarine to subaerial eruption occurs at ~710 m below present sea level and 2.5 Ma. Since 2.5 Ma, there has been ~520 m of subsidence over and above the expected ~190 m due to lithospheric cooling. Plausible elastic thicknesses and growth histories would generate a maximum elastic subsidence since 2.5 Ma of ~200 m. We infer that the subsidence includes a component of viscous relaxation resulting from rapid loading prior to 2.5 Ma, and place constraints on the timescale of this relaxation, and hence the viscosity of the underlying lithosphere.

1. Introduction

The growth of volcanic ocean islands places a time-varying load on the lithosphere, and the response of the lithosphere to that load provides information about lithospheric rheology. Over long timescales, to a good approximation, the lithosphere behaves like a thin elastic plate and the response may be characterized by a single parameter, the effective elastic thickness [e.g., *Calmant et al.*, 1990; *Watts and Cochran*, 1974]. However, on shorter timescales there is a viscous component to the response [e.g., *Walcott*, 1970]. This component may be parameterized by considering the response of a thin visco-elastic sheet on an inviscid substrate [e.g., *Lambeck and Nakiboglu*, 1981], or alternatively by a model in which viscosity varies more smoothly with temperature and hence depth [e.g., *Courtney and Beaumont*, 1983; *Watts and Zhong*, 2000]. If the timing of load emplacement is sufficiently well known, subsidence rates of volcanic islands can provide constraints on this viscous behavior [e.g., *Watts and Zhong*, 2000]. Although subsidence rates may be measured on geological timescales through coral growth rates [e.g., *Moore et al.*, 1996] or dating of submerged terraces, volcanic loading histories are usually poorly known. However, the dating of material from deep boreholes in ocean islands can allow constraints to be placed not only on the growth rate but also, through measurement of the depth and age of the submarine-subaerial transition, the long-term subsidence rate [*Hyndman et al.*, 1979; *Sharp and Renne*, 2005]. Here we use such measurements from Ascension Island in the central Atlantic to investigate the response of young oceanic lithosphere to volcanic loading.

2. Isotopic Dating of Borehole Samples

Ascension Island forms the summit of a ~4-km-high volcanic edifice lying on 7 Ma oceanic lithosphere, 90 km west of the mid-Atlantic Ridge (Fig. 1). K-Ar dating of surface samples has yielded ages of up to 1.5 Ma, while sparse Ar-Ar geochronology has yielded ages of 0.4-1.0 Ma. [*Harris et al.*, 1982; *Kar et al.*, 1998; *Nielson and Sibbett*, 1996]. A tomographic seismic experiment showed that the lower oceanic crust is thickened beneath the island but no evidence of a velocity discontinuity between pre-existing crust and a magmatic “underplate”, leading to the suggestion that the bulk of the volcanic edifice may have formed close to the ridge axis [*Evangelidis et al.*, 2004; *Klingelhoefer et al.*, 2001]. The Ascension #1(ASC-1) borehole was drilled to a depth of 3.1 km as part of a geothermal exploration project, which also drilled several shallower boreholes [*Nielson and Stiger*, 1996]. The borehole was not cored, but cuttings were collected for each 3-m depth interval and archived. Most of the cutting material consisted of heavily altered volcanic dust, but some larger and fresh fragments were also available. Basaltic to doleritic clasts of well-crystallized glass-free fresh groundmass 1-2 in cm size were dated using the $^{40}Ar/^{39}Ar$ laser-heating technique. At each depth only clasts of most dominant rock type which clearly represents the lithofacies at the sampling depth were considered for analysis. Age determinations were conducted using $^{40}Ar/^{39}Ar$ geochronology facility at the Geological Survey of Japan/AIST [*Ishizuka et al.*, 2003; *Ishizuka et al.*, 2009]. Details of analytical procedure are described in the electronic supplement.

Samples from four different depths of the ASC-1 gave plateau ages. Two fragments from a single sample from 834-837 m depth (all depths are relative to the kelly bushing at 181 m above sealevel) were analyzed separately, and returned identical plateau ages (2.43±0.07 and 2.42±0.09 Ma). This result demonstrates the high reproducibility of the analysis on small amount of cuttings material. Two different samples from 894-897m depth returned well-defined plateau ages of 2.23±0.07 and 2.48±0.10 Ma, respectively. These plateau ages are also identical within 2σ error. In between these depths, the shallowest hyaloclastite section (which was erupted in a submarine environment) was recovered between 887 and 939 m depth [*Nielson and Stiger*, 1996], and 887 m marks the transition from subaerial to submarine eruption, which is therefore dated accurately. A sample from 1050-1053m depth gave a similar plateau age of 2.5±0.3 Ma. A clast from 1233-1236 m depth yielded a partly disturbed age spectrum with a significantly older plateau age of 3.41±0.25 Ma. Inverse isochrons for each plateau obtained here gave Ar initial ratios identical to atmospheric ratio within 2σ error, indicating no presence of extraneous Ar. No samples suitable for analysis were found outside the depth range 834-1236 m.

3. Modeling the Growth and Subsidence of Ascension Island

The radiometric dates show that the volcanic edifice is indeed much older than indicated by surface samples, that substantial subsidence has occurred since 2.5 Ma, and that the mean volcanic growth rate during that period has been ~0.4 km/My (Fig. 3). First, we explored whether this subsidence could be adequately explained by an elastic response. We calculated the flexural isostatic response to three possible loading scenarios, using the load volume defined by *Evangelidis et al.* [2004] and load and infill densities of 2323 kg/m^3 based on the seismic velocity structure of the volcanic edifice [*Evangelidis et al.*, 2004]. The mantle density was 3330 kg/m^3. In each scenario, it is assumed that any space created by flexural subsidence is filled by new igneous material, and vertical distances are rounded to the nearest

10 m. In scenario 1, all the currently subaerial load has been added since 2.5 Ma. In scenario 2, the growth rate of the volcanic edifice is in proportion to its current height, such that 180 m of load has been added at the borehole location and no new material has been added around the perimeter of the volcanic edifice. In scenario 3, a 180 m layer of load has been added at all locations, except where the current edifice is less than 180 m high, where the whole of the edifice has been added since 2.5 Ma.

Analysis of both gravity and seismic data indicate that the lithosphere has significant flexural strength, with an effective elastic thickness T_e of 2-4 km inferred from gravity data [*Minshull and Brozena*, 1997] and a value of at least 6 km inferred from the Moho shape derived from wide-angle seismic data [*Evangelidis et al.*, 2004]. Both estimates involve assumptions about the processes controlling the shape of the Moho depression beneath the island, but the latter estimate involves fewer assumptions and is therefore more reliable. For a T_e of 6 km, the maximum subsidence predicted since 2.5 Ma is 110 m (Fig. 3). Even if we assume a T_e of as low as 1 km, the elastic subsidence predicted since 2.5 Ma is 130 m, 220 m and 280 m for scenarios 1-3, respectively. Ignoring eustatic sea-level changes, which cannot be accounted for given the age uncertainties for the subaerial to submarine transition, the observed subsidence is 710 m, There are 600-700 m of additional subsidence to explain for a 6 km elastic thickness, or 430-580 m for 1 km elastic thickness. Some of this additional subsidence might be explained by thermal subsidence since 2.5 Ma. However, if the lithosphere has subsided according to plate cooling models [*Stein and Stein*, 1992], only ~190 m of subsidence is predicted between ages of 4.5 and 7.0 My. There is no significant residual depth anomaly in the surrounding lithosphere [*Minshull et al.*, 1998], so there is no evidence for anomalous thermal subsidence. Some vertical motion may arise from flexural bending associated with the adjacent Ascension Fracture Zone, but the island is ~60 km from this fracture zone, so such motion is likely to be small. Anomalous subsidence might be attributed to removal of dynamic support associated with an "Ascension plume", but the timescale required is very short for such a large-scale event. Hence we must seek an alternative explanation for the large subsidence observed.

The anomalous subsidence might be explained if a viscous component leads to a delay between volcanic loading and the isostatic response of the lithosphere. *Watts and Zhong* [2000] infer from observations of flexural rigidity D as a function of both plate age and load age that under volcanic loading, the oceanic lithosphere responds as a medium with viscosity decaying gradually with depth as temperature increases. The simplest possible model capturing the isostatic, elastic and viscous response of the lithosphere to vertical loads is the thin viscoelastic plate model, which incorporates the widely used flexural response plus a time-dependent viscous relaxation due to a vertically-averaged lithosphere viscosity. We extended our analysis to include a viscous component by using the finite-difference code TISC [*Garcia-Castellanos*, 2002], which calculates the vertical deflection *w(x,y)* of a viscoelastic thin plate when submitted to a load distribution *q(x,y)*. The deflection has two components: an instantaneous elastic response and a subsequent deflection velocity *dw/dt* related to viscous stress relaxation. In the absence of horizontal forces and lateral rigidity variations the elastic component can be calculated with the following equation [*van Wees and Cloetingh*, 1994]:

$$D\frac{\partial^4 w}{\partial x^4} + D\frac{\partial^4 w}{\partial y^4} + 2D\frac{\partial^4 w}{\partial x^2 \partial y^2} + \Delta\rho\, g\, w = q(x,y)$$

where υ is Poisson's ratio (assumed to be 0.25) and $\Delta\rho$ is the density difference between sublithospheric mantle and the infill. Load and infill densities were as for the elastic calculation above. D is calculated from T_e assuming a Young's modulus of $7\text{x}10^{10}$ Pa [e.g., *Panteleyev and Diament*, 1993]. To calculate the viscous component of the deflection, the same equation is solved but *w* is replaced by *dw/dt*, υ is 0.5, *q* is replaced by $(q - \Delta\rho \cdot g \cdot w)/\tau$, where τ is the viscous relaxation time, and the total deflection is computed by integrating over time.

The viscous flexural equation predicts that the deflection tends towards local isostatic equilibrium (similar to a reduction of T_e through time for an elastic plate) at timescales similar to τ, which relates to viscosity μ through $\tau = 2(1 + \nu)\mu/E$. We solved both equations (the elastic and the viscous one) for a range of values of T_e and τ, and for two different loading histories (Fig. 4). In both, we assume loading according to scenario 2, such that 12% of the load has been added since 3.4 Ma. In the first, we assumed the remainder of the loading occurred through rapid volcano growth at 5 Ma, and in the second we assumed that this loading occurred at 4 Ma. For loading at 5 Ma, the maximum predicted subsidence since 2.5 Ma is less than 500 m (Fig. 4a), so insufficient to account for the 520 m difference between the observed subsidence and the predicted thermal subsidence. For loading at 4 Ma, the predicted subsidence since 2.5 Ma exceeds 500 m for T_e values of ~3-7 km and τ values of ~0.5-1.0 My (Fig. 4b), corresponding to a viscosity of ~$0.4\text{-}0.7\text{x}10^{24}$ Pa s.   For lower values of τ, the subsidence is largely complete before 2.5 Ma, while for higher values the subsidence is too slow. For higher values of T_e, there is too little subsidence to match the observations, while for lower values, although the overall subsidence is greater, it becomes focused at earlier times and the subsidence since 2.5 Ma is too small. These results also suggest that the main loading event cannot have occurred much before 5 Ma (because then subsidence would be largely complete by 2.5 Ma), and the borehole data suggest that it cannot have occurred after 3.4 Ma.

4. Discussion and Conclusions

The observed growth rate of Ascension Island since 3.4 Ma of 0.4 km/My is very similar to the post-shield growth rate of 0.9 km/My inferred from $^{40}Ar/^{39}Ar$ dating of borehole samples from the Hawaii Scientific Drilling Project, and an order of magnitude less than the 8.6 km/My growth rate of Mauna Kea during its shield-building phase [*Sharp and Renne*, 2005]. The mean subsidence rate of 0.3 km/My since 2.5 Ma is much smaller than the 2.6 km/My value inferred at Hawaii [*Sharp and Renne*, 2005]. Both observations place Ascension Island well into its post-shield phase, consistent with the evolved composition of most outcropping volcanic rocks [e.g., *Kar et al.*, 1998], and isotopic evidence that the shield-building phase was fed by a different magma reservoir than the rocks that outcrop at the surface [*Paulick et al.*, 2010]. During the shield-building phase, the volcano was only 30-40 km from the ridge axis, in a similar location to a present-day subcircular caldera identified by *Klingelhoefer et al.* [2001].

Both elastic and visco-elastic models would predict a bowl-shaped depression of the Moho beneath the edifice. Whilst there is some evidence from seismic data that the Moho deepens beneath Ascension, the depression is far from bowl-shaped and rather appears to be elongated in an east-west direction [*Evangelidis et al.*, 2004]. However, the observation that substantial subsidence occurs > 1 My after the main shield-building phase of volcano growth requires a time constant on the order of 1 My for a visco-elastic model and therefore the inferred value of lithospheric viscosity is robust (within a factor of 2-3) whatever the precise details of the growth history and nature of magmatic addition. However, given that significant lithospheric cooling likely occurred during volcano growth, the viscosity may also have changed significantly, so that the inferred value will be a time-averaged value.

We conclude the following:

1. Ascension Island has a complex growth history that is not revealed by surface sampling.
2. For plausible growth histories, the subsidence at the ASC#1 borehole cannot be explained by elastic models.
3. The main volcanic edifice has been built during the period 5.0-3.4 Ma.
4. The viscoelastic component of subsidence is consistent with a relaxation time of ~0.5-1.0 My and a lithosphere viscosity of 0.4-0.7x 10^{24} Pa s.

Acknowledgments

We thank Dennis Nielson and David Langton (University of Utah) for assisting us to sample the borehole material. We thank two anonymous reviewers for constructive comments.

Figure captions

Figure 1. Topography of Ascension Island and the location of the ASC-1 borehole. White lines mark the magnetic anomaly picks of *Brozena* [1986]. Inset shows the tectonic setting of the island on the west flank of the Mid-Atlantic Ridge.

Figure 2. $^{40}Ar/^{39}Ar$ age spectra with Ca/K plot for groundmass samples of basaltic rocks drilled from the ASC#1 borehole on the Ascension Island. Error for each step is given at the 1σ level. Plateau ages were calculated as weighted means of ages of plateau-forming steps, where each age was weighted by the inverse of its variance.

Figure 3. a) Circles mark ages and present-day depths below sea-level of ASC1 borehole samples, with uncertainties. Thick bar marks age range of surface samples. Dotted lines mark present-day sea-level and estimated depth of subaerial to submarine transition. Dashed line indicates approximate mean island growth rate since 3.4 Ma. b) Predicted elastic subsidence since 2.5 Ma, at the borehole site, for the three island growth scenarios described in the text and a range of effective elastic thicknesses (T_e). Solid, dotted and dashed lines correspond to scenarios 1, 2 and 3, respectively. Vertical line marks the lower limit on T_e inferred by [*Evangelidis et al.*, 2004]

Figure 4. Predicted visco-elastic subsidence at the borehole site since 2.5 Ma for two different loading histories. a) 88% of load emplaced at 5 Ma and 12% since 3.4 Ma. b) 88% of load emplaced at 4 Ma and 12% since 3.4 Ma.

References

Brozena, J. M. (1986), Temporal and spatial variability of seafloor spreading processes in northern South Atlantic, *Journal of Geophysical Research*, *91*(B1), 497-510.

Calmant, S., et al. (1990), Elastic layer thickening with age of the oceanic lithosphere; a tool for prediction of the age of volcanoes or oceanic crust, *Geophysical Journal International*, *100*(1), 59-67.

Courtney, R. C., and C. Beaumont (1983), Thermally-activated creep and flexure of the oceanic lithosphere, *Nature*, *305*(5931), 201-204.

Evangelidis, C. P., et al. (2004), Three-dimensional crustal structure of Ascension Island from active source seismic tomography, *Geophysical Journal International*, *159*(1), 311-325.

Garcia-Castellanos, D. (2002), Interplay between lithospheric flexure and river transport in foreland basins, *Basin Research*, *14*(2), 89-104.

Harris, C., et al. (1982), Isotopic composition of lead and strontium in lavas and coarse-grained blocks from Ascension Island, South Atlantic; an addendum, *Earth and Planetary Science Letters*, *63*(1), 139-141.

Hyndman, R. D., et al. (1979), Seismic velocities, densities, electrical resistivities, porosities and thermal conductivities of core samples from boreholes into the islands of Bermuda and the Azores, *Maurice Ewing Series, no*, *2*, 94-112.

Ishizuka, O., et al. (2003), Volcanic history of the back-arc region of the Izu-Bonin (Ogasawara) arc, *Spec. Publ. Geol. Soc. London*, *219*, 187-205.

Ishizuka, O., et al. (2009), Two contrasting magmatic types coexist after the cessation of back-arc spreading, *Chemical Geology*, *266*, 283-305.

Kar, A., et al. (1998), Origin of differentiated volcanic and plutonic rocks from Ascension Island, South Atlantic Ocean, *Journal of Petrology*, *39*(5), 1009-1024.

Klingelhoefer, F., et al. (2001), Crustal structure of Ascension Island from wide-angle seismic data; implications for the formation of near-ridge volcanic islands, *Earth and Planetary Science Letters*, *190*(1-2), 41-56.

Lambeck, K., and S. M. Nakiboglu (1981), Seamount loading and stress in the ocean lithosphere; 2, Viscoelastic and elastic-viscoelastic models, *Journal of Geophysical Research*, *86*(B8), 6961-6984.

Minshull, T. A., and J. M. Brozena (1997), Gravity anomalies and flexure of the lithosphere at Ascension Island, *Geophysical Journal International*, *131*(2), 347-360.

Minshull, T. A., et al. (1998), Ridge-plume interactions or mantle heterogeneity near Ascension Island?, *Geology*, *26*(2), 115-118.

Moore, J. G., et al. (1996), Coral ages and island subsidence, Hilo drill hole, *Journal of Geophysical Research*, *101*(B5), 11,599-511,605.

Nielson, D. L., and B. S. Sibbett (1996), Geology of Ascension Island, South Atlantic Ocean, *Geothermics*, *25*(4-5), 427-448.

Nielson, D. L., and S. G. Stiger (1996), Drilling and evaluation of Ascension #1; a geothermal exploration well on Ascension Island, South Atlantic Ocean, *Geothermics*, *25*(4-5), 543-560.

Panteleyev, A. N., and M. Diament (1993), Influence of some rheological parameters on flexure of the oceanic lithosphere, *Geophysical Journal International*, *114*(1), 209-220.

Paulick, H., et al. (2010), The influence of small-scale mantle heterogeneities on Mid-Ocean Ridge volcanism: Evidence from the southern Mid-Atlantic Ridge (7°30'S to 11°30"S) and Ascension Island, *Earth and Planetary Science Letters*, *296*, 3-4.

Sharp, W. D., and P. R. Renne (2005), The ^{40}Ar/^{39}Ar dating of core recovered by the Hawaii Scientific Drilling Project (phase 2), Hilo, Hawaii, *Geochemistry, Geophysics, Geosystems*, *6*, Q04G17, doi:10.1029/2004GC000846

Stein, C. A., and S. Stein (1992), A Model for the Global Variation in Oceanic Depth and Heat-Flow with Lithospheric Age, *Nature*, *359*(6391), 123-129.
van Wees, J. D., and S. Cloetingh (1994), A finite-difference technique to incorporate spatial variations in rigidity and planar faults into 3-D models for lithospheric flexure, *Geophysical Journal International*, *117*(1), 179-195.
Walcott, R. I. (1970), Flexural rigidity, thickness, and viscosity of the lithosphere, *Journal of Geophysical Research*, *75*(20), 3941-3954.
Watts, A. B., and J. R. Cochran (1974), Gravity Anomalies and Flexure of the Lithosphere along the Hawaiian-Emperor Seamount Chain, *Geophysical Journal of the Royal Astronomical Society*, *38*(1), 119-141.
Watts, A. B., and S. Zhong (2000), Observations of flexure and the rheology of oceanic lithosphere, *Geophysical Journal International*, *142*(3), 855-875.

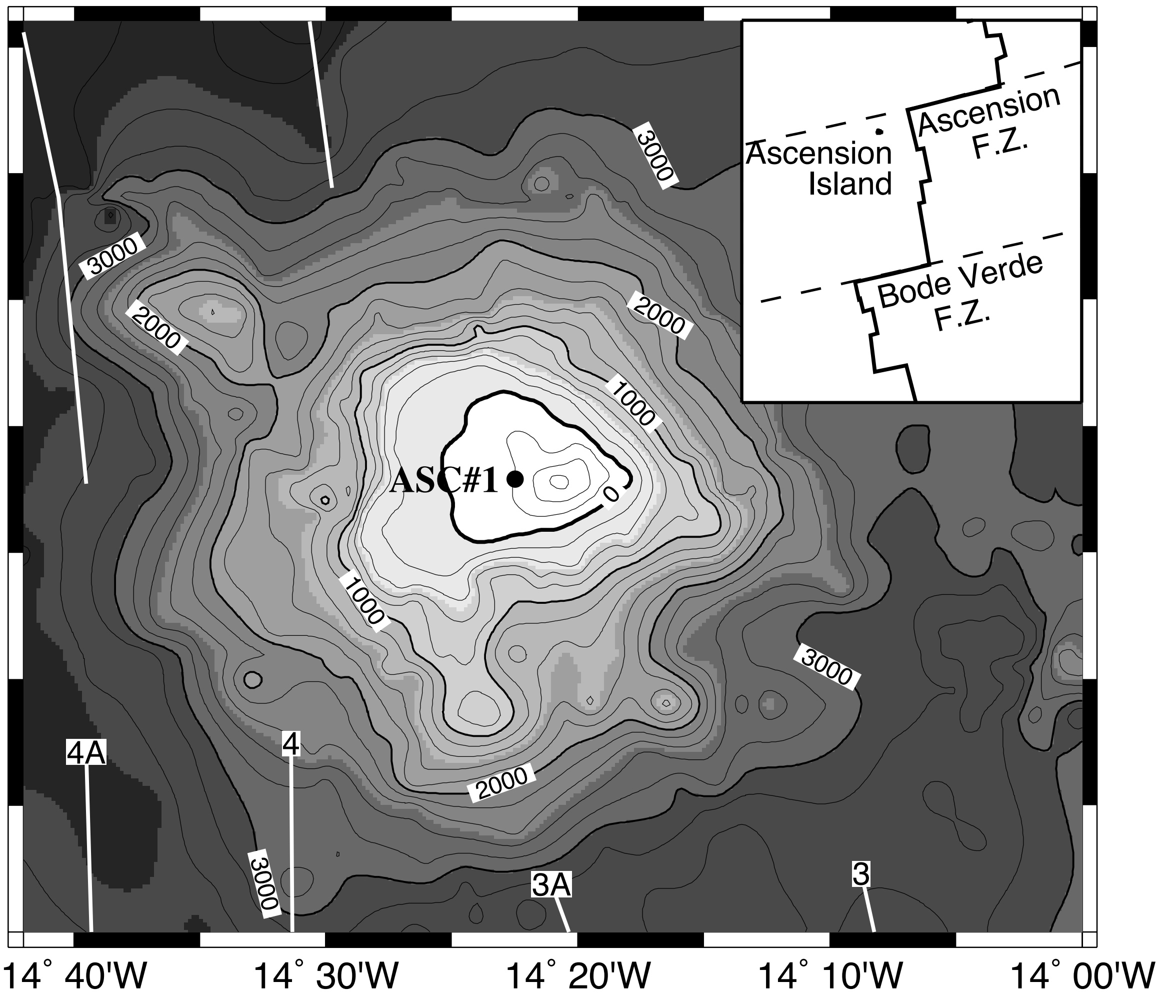

Minshull et al. Fig. 1

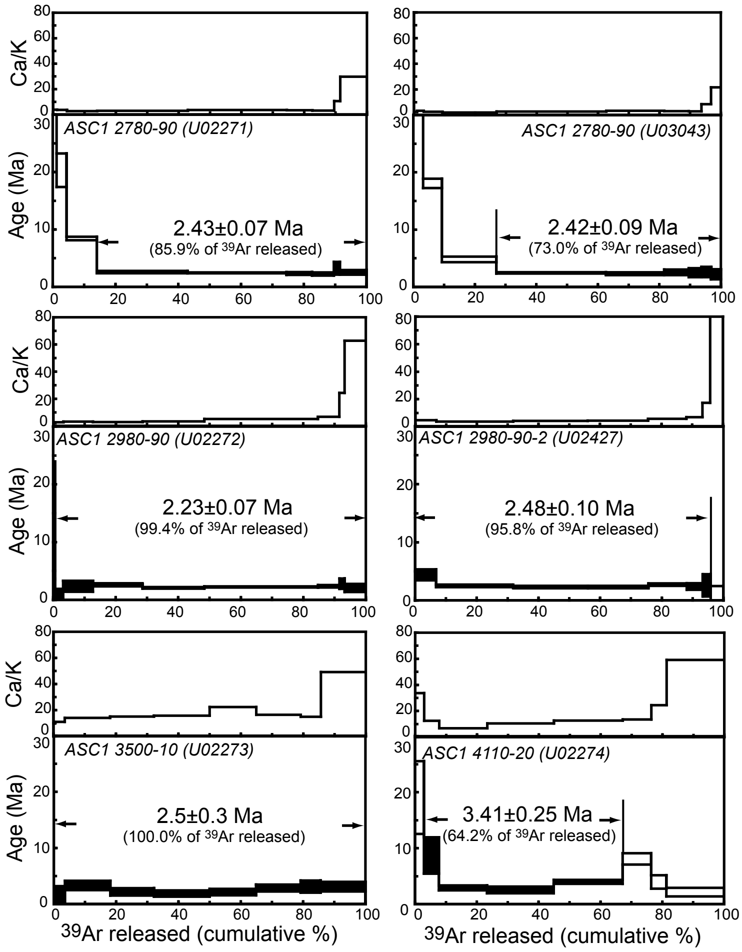

Minshull et al. Fig. 2

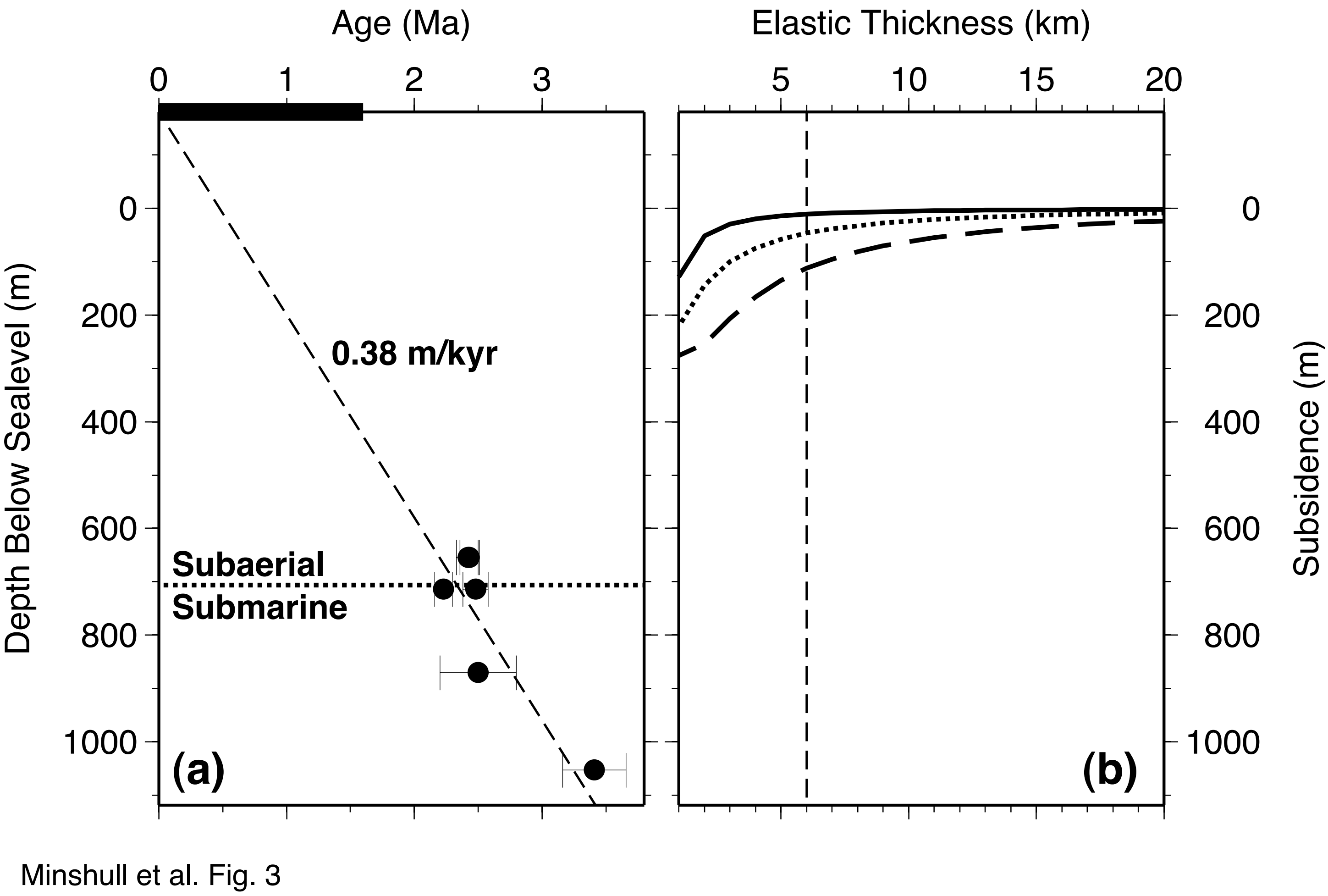

Minshull et al. Fig. 3

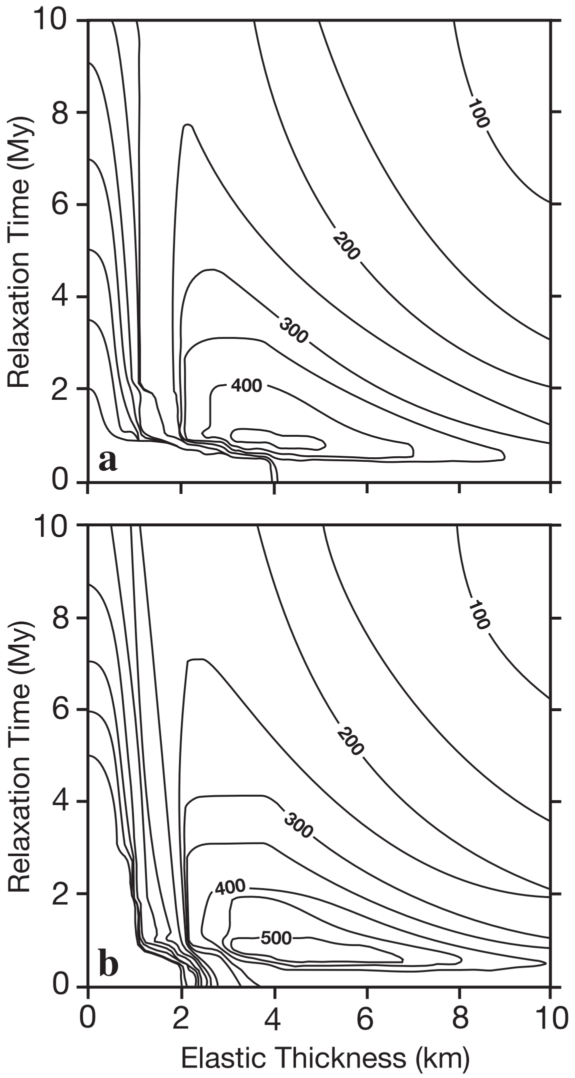

Minshull et al, fig. 4

Dating method

Age determinations were conducted using $^{40}Ar/^{39}Ar$ geochronology facility at the Geological Survey of Japan/AIST. Laser step-heating experiments were conducted on 6.6-10.3 mg groundmass samples. We analysed on a groundmass separate from a single chip of drill cuttings. Slabs 1 mm-thick were taken out from the freshest part of the samples with a water-cooled saw. This is partly because flat surfaces are required to precisely monitor the thermal energy distribution on the samples during laser heating. The slabs were gently crushed into small pieces of about 0.5-1 mg weight. The samples were treated ultrasonically in 3N HCl for 30 minutes and then 4N HNO_3 for 30 minutes to remove possible alteration products (clays and carbonates) prior to irradiation. After this acid treatment, groundmass separate was prepared under binocular microscope by handpicking. Sanidine separated from the Fish Canyon Tuff (FC3) was used for the flux monitor and assigned an age of 27.5 Ma [*Lanphere and Baadsgaard*, 2001].

Samples were baked at 250°C for 72 hours after being placed in an extraction line before analysis. A continuous Ar ion laser was used for sample heating. The groundmass samples were heated for 3 minutes in each step keeping laser power constant. Laser beam diameter was adjusted to 2 mm to ensure uniform heating of the sample. Extracted gas was purified for 10 minutes with three Zr-Al getters (SAES AP-10) and one Zr-Fe-V getter (SAES GP-50). Two Zr-Al getters were maintained at 400°C and other getters were at room temperature. Argon isotopes were measured on a VG Isotech VG3600 noble gas mass spectrometer fitted with a BALZERS electron multiplier. The sensitivity of the collector was about 5×10^{-10} ml STP/V. Mass discrimination was monitored using diluted air.

Correction for interfering isotopes was achieved by analyses of $CaFeSi_2O_6$ and $KFeSiO_4$ glasses irradiated with the samples. The blank of the system including the mass spectrometer and the extraction line was 7.5 x 10^{-14} ml STP for ^{36}Ar, 2.5 x 10^{-13} ml STP for ^{37}Ar, 2.5 x 10^{-13} ml STP for ^{38}Ar, 1.0 x 10^{-12} ml STP for ^{39}Ar and 2.5 x 10^{-12} ml STP for ^{40}Ar. A blank analysis was done every 2 or 3 steps of the analyses.

All errors for ^{40}Ar/^{39}Ar results are reported at one standard deviation. Errors for ages include analytical uncertainties for Ar isotope analysis, correction for interfering isotopes and J value estimation. An error of 0.5 % was assigned to J values as a pooled estimate during the course of this study. The age plateaus were determined following the definition by *Fleck et al.* [1977]. Inverse isochrones (Fig. A1) were calculated using York's least-squares fit, which accommodates errors in both ratios and correlations of errors [*York*, 1969].

Results from the analyses are tabulated in Tables A1 and A2 and inverse isochron plots are shown in Figure A1.

Figure Caption

Fig. A1. Inverse isochron plots for groundmass samples of volcanic rocks from the ASC1 drilling site on the Ascension Island. Solid symbols in the inverse isochron plots are the steps used for isochron (plateau forming steps). Error bar for each step is given at the 1σ level.

References

Fleck, R. J., et al. (1977), Interpretation of discordant (super 40) Ar/ (super 39) Ar age-spectra of Mesozoic tholeiites from Antarctica, *Geochimica et Cosmochimica Acta*, *41*(1), 15-32.

Lanphere, M. A., and H. Baadsgaard (2001), Precise K-Ar, (super 40) Ar/ (super 39) Ar, Rb-Sr and U/Pb mineral ages from the 27.5 Ma Fish Canyon Tuff reference standard, *Chemical Geology*, *175*(3-4), 653-671.

York, D. (1969), Least squares fitting of a straight line with correlated errors, *Earth and Planetary Science Letters*, *5*(5), 320-324.

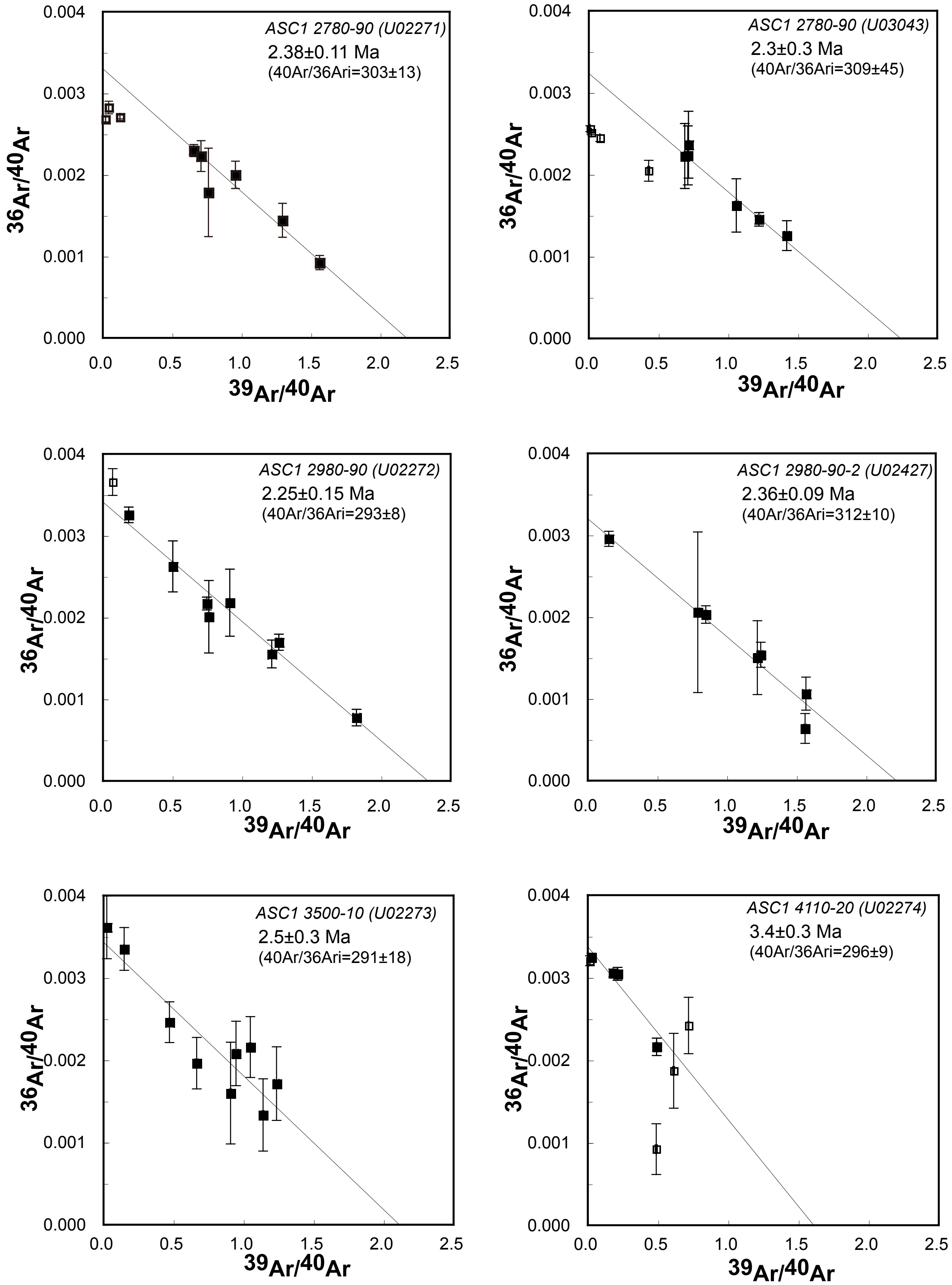

Minshull et al. Fig. A1

Table A1: Results of stepwise-heating analyses of volcanic rocks from the ASC1 drilling site on the Ascension Island.

Analysis No.	Sample No.	depth from surface (m)	Total age (±1σ) integrated age (Ma)	Plateau age (±1σ) weighted average (Ma)	inv. isochron age (Ma)	$^{40}Ar/^{36}Ar$ intercept	MSWD	fraction of ^{39}Ar (%)
U02271	ASC1 2780-90	834-837	4.25±0.13	**2.43±0.07**	2.38±0.11	303±13	0.60	85.9
U03043	ASC1 2780-90	834-837	6.78±0.16	**2.42±0.09**	2.3±0.3	309±45	0.32	73.0
U02272	ASC1 2980-90	894-897	2.22±0.12	**2.23±0.07**	2.25±0.15	293±8	1.08	99.4
U02427	ASC1 2980-90-2	894-897	2.45±0.16	**2.48±0.10**	2.36±0.09	312±10	0.92	95.8
U02273	ASC1 3500-10	1050-1053	2.52±0.29	**2.5±0.3**	2.5±0.3	291±18	0.89	100.0
U02274	ASC1 4110-20	1233-1236	4.22±0.35	**3.41±0.25**	3.4±0.3	296±9	2.10	64.2

Table A2

Results of isotopic analysis for $^{40}Ar/^{39}Ar$ dating of samples from the ASC1 drilling site on Ascension Island																		
Laser output	$^{40}Ar/^{39}Ar$			$^{37}Ar/^{39}Ar$			$^{36}Ar/^{39}Ar$ ($x10^{-3}$)			K/Ca	$^{40}Ar^*$ (%)	$^{39}Ar_K$ fraction (%)	$^{40}Ar^*/^{39}Ar_K$			Age(±1σ) (Ma)		
ASC1 2780-90	*ASC1 2780-90*																	
J=	0.002896																	
0.6W	50.05	±	0.51	2.254	±	0.025	135.1	±	1.7	0.26	20.8	1.2	10.41	±	0.53	54	±	3
0.92W	23.64	±	0.33	2.176	±	0.042	67.59	±	1.86	0.27	16.5	3.2	3.912	±	0.565	20	±	3
1.3W	8.074	±	0.038	1.597	±	0.015	22.45	±	0.20	0.37	20.0	9.6	1.614	±	0.059	8.4	±	0.3
1.75W	1.525	±	0.022	1.750	±	0.023	4.146	±	0.112	0.34	32.1	28.9	0.4901	±	0.0355	2.56	±	0.19
2.1W	0.6388	±	0.0025	2.119	±	0.009	1.368	±	0.050	0.28	72.7	31.6	0.4653	±	0.0164	2.43	±	0.09
2.48W	0.7709	±	0.0032	2.018	±	0.009	1.852	±	0.159	0.29	57.4	8.1	0.4433	±	0.0476	2.31	±	0.25
3.13W	1.045	±	0.004	1.844	±	0.015	2.767	±	0.173	0.32	40.9	6.9	0.4279	±	0.0517	2.2	±	0.3
4.05W	1.306	±	0.010	6.218	±	0.038	4.615	±	0.705	0.09	47.2	1.9	0.6203	±	0.2106	3.2	±	1.1
fusion	1.393	±	0.005	17.23	±	0.05	9.435	±	0.186	0.03	34.1	8.5	0.4821	±	0.0789	2.5	±	0.4
ASC1 2780-90	*U03043*																	
J=	0.002896																	
0.6W	106.9	±	1.0	1.403	±	0.199	274.1	±	4.3	0.42	24.4	1.0	26.07	±	1.24	131	±	6
0.92W	56.37	±	0.34	1.990	±	0.109	142.4	±	1.7	0.30	25.7	2.2	14.53	±	0.47	74	±	2
1.3W	12.51	±	0.06	1.505	±	0.034	31.16	±	0.53	0.39	27.7	6.1	3.475	±	0.157	18	±	1
1.53W	2.327	±	0.039	1.184	±	0.020	5.197	±	0.295	0.50	39.5	17.7	0.9203	±	0.0906	4.8	±	0.5
2.1W	0.8176	±	0.0079	1.622	±	0.015	1.784	±	0.066	0.36	57.1	35.7	0.4672	±	0.0211	2.44	±	0.11
2.48W	0.7031	±	0.0084	1.924	±	0.030	1.589	±	0.126	0.31	62.9	18.9	0.4431	±	0.0385	2.31	±	0.20
2.1W	0.9442	±	0.0056	1.797	±	0.024	2.193	±	0.306	0.33	52.0	8.0	0.4921	±	0.0910	2.6	±	0.5
2.45W	1.406	±	0.009	1.716	±	0.046	3.772	±	0.505	0.34	34.0	4.1	0.4783	±	0.1499	2.5	±	0.8
3W	1.446	±	0.012	4.951	±	0.099	5.037	±	0.570	0.12	34.2	3.1	0.4969	±	0.1704	2.6	±	0.9
fusion	1.383	±	0.010	12.54	±	0.07	7.872	±	0.548	0.05	30.1	3.2	0.4213	±	0.1689	2.2	±	0.9
ASC1 2980-90	*U02272*																	
J=	0.002913																	
0.6W	14.49	±	0.26	1.341	±	0.047	53.48	±	2.38	0.44	0.0	0.6	0.0002	±	0.6953	0.0	±	3.7
0.92W	5.403	±	0.063	1.591	±	0.022	18.17	±	0.52	0.37	3.8	2.6	0.2078	±	0.1528	1.1	±	0.8
1.3W	1.990	±	0.022	1.871	±	0.027	5.909	±	0.621	0.31	22.5	9.5	0.4481	±	0.1838	2.4	±	1.0
1.75W	1.337	±	0.022	1.674	±	0.024	3.513	±	0.105	0.35	35.9	15.9	0.4806	±	0.0338	2.52	±	0.18
2.1W	0.7896	±	0.0115	2.031	±	0.027	2.085	±	0.076	0.29	49.9	19.8	0.3945	±	0.0244	2.07	±	0.13
2.48W	0.5471	±	0.0071	3.004	±	0.036	1.527	±	0.046	0.20	77.1	36.3	0.4229	±	0.0176	2.22	±	0.09
3.15W	0.8211	±	0.0031	3.976	±	0.014	2.734	±	0.133	0.15	54.1	6.9	0.4461	±	0.0414	2.34	±	0.22

Table A2

3.9W	1.297	±	0.019	14.15	±	0.16	7.800	±	0.557	0.04	40.7	1.7	0.5341	±	0.1726	2.8	±	0.9
fusion	1.063	±	0.004	35.81	±	0.11	15.47	±	0.20	0.02	35.6	6.8	0.3904	±	0.1330	2.1	±	0.7
ASC1 2980-90-2	*U02427*																	
J=	0.002904																	
0.6W	6.615	±	0.095	2.809	±	0.039	20.59	±	0.62	0.21	12.6	6.8	0.8385	±	0.1840	4.4	±	1.0
0.95W	1.178	±	0.013	2.214	±	0.022	3.205	±	0.124	0.27	40.0	25.0	0.4723	±	0.0384	2.47	±	0.20
1.25W	0.8032	±	0.0095	2.478	±	0.028	2.146	±	0.120	0.24	54.5	24.2	0.4389	±	0.0371	2.30	±	0.19
1.6W	0.6366	±	0.0100	2.603	±	0.032	1.632	±	0.126	0.23	68.6	19.6	0.4378	±	0.0391	2.29	±	0.20
2.1W	0.6386	±	0.0042	3.313	±	0.017	1.624	±	0.111	0.18	81.2	12.5	0.5199	±	0.0347	2.72	±	0.18
2.7W	0.8175	±	0.0112	4.035	±	0.046	2.711	±	0.366	0.15	55.6	5.2	0.4559	±	0.1098	2.4	±	0.6
4.1W	1.255	±	0.020	10.07	±	0.11	6.281	±	1.227	0.06	39.2	2.5	0.4963	±	0.3674	2.6	±	1.9
fusion	1.465	±	0.026	47.84	±	0.53	24.41	±	1.44	0.01	0.0	4.2	0.0001	±	0.4694	0.0	±	2.5
ASC1 3500-10	*U02273*																	
J=	0.002985																	
0.6W	42.69	±	1.08	5.748	±	0.194	156.4	±	16.7	0.10	0.0	0.4	0.0011	±	4.8459	0.0	±	26.1
0.95W	6.772	±	0.077	6.416	±	0.084	25.04	±	1.77	0.09	1.0	3.2	0.0680	±	0.5232	0.4	±	2.8
1.4W	1.492	±	0.021	8.255	±	0.092	5.961	±	0.459	0.07	42.0	14.5	0.6312	±	0.1394	3.4	±	0.7
1.8W	1.049	±	0.016	8.853	±	0.105	5.435	±	0.401	0.07	38.5	14.0	0.4070	±	0.1227	2.2	±	0.7
2.3W	0.9470	±	0.0057	9.203	±	0.049	5.424	±	0.335	0.06	36.2	17.9	0.3458	±	0.1042	1.9	±	0.6
2.8W	0.8000	±	0.0103	12.98	±	0.13	6.138	±	0.331	0.04	49.3	14.9	0.3992	±	0.1073	2.1	±	0.6
3.4W	0.8703	±	0.0055	9.617	±	0.046	4.692	±	0.368	0.06	60.6	14.3	0.5319	±	0.1140	2.9	±	0.6
4.05W	1.094	±	0.007	8.723	±	0.041	4.953	±	0.670	0.07	52.7	6.4	0.5814	±	0.2015	3.1	±	1.1
fusion	2.075	±	0.009	28.21	±	0.10	15.47	±	0.41	0.02	27.3	14.4	0.5805	±	0.1556	3.1	±	0.8
ASC1 4110-20	*U02274*																	
J=	0.003012																	
0.6W	65.64	±	1.03	19.45	±	0.29	217.6	±	4.5	0.03	5.3	2.9	3.526	±	1.209	19.1	±	6.5
0.95W	38.49	±	0.45	7.286	±	0.098	127.5	±	2.1	0.08	4.1	4.8	1.606	±	0.599	8.7	±	3.2
1.4W	5.508	±	0.051	3.912	±	0.039	18.27	±	0.26	0.15	9.7	15.6	0.5354	±	0.0788	2.9	±	0.4
1.8W	4.715	±	0.050	6.096	±	0.062	16.60	±	0.37	0.10	10.0	21.5	0.4720	±	0.1104	2.6	±	0.6
2.3W	2.026	±	0.028	7.427	±	0.096	7.105	±	0.203	0.08	36.1	22.3	0.7368	±	0.0657	4.0	±	0.4
2.8W	2.037	±	0.031	7.832	±	0.094	4.756	±	0.622	0.07	72.7	9.2	1.492	±	0.188	8.1	±	1.0
3.85W	1.616	±	0.018	14.23	±	0.12	8.252	±	0.719	0.04	44.7	4.9	0.7311	±	0.2199	4.0	±	1.2
fusion	1.354	±	0.005	33.71	±	0.13	15.66	±	0.29	0.02	28.5	18.7	0.3972	±	0.1408	2.2	±	0.8